Available online at www.sciencedirect.com
ScienceDirect
Trans. Nonferrous Met. Soc. China 29(2019) 15−24
Transactions of Nonferrous Metals Society of China
www.tnmsc.cn

Distribution and evolution of aging precipitates in Al−Cu−Li alloy with high Li concentration

Jin-feng LI[1,2,3], Jia-lei HUANG[1], Dan-yang LIU[1], Yong-lai CHEN[4], Xu-hu ZHANG[4], Peng-cheng MA[4]

1. School of Materials Science and Engineering, Central South University, Changsha 410083, China;
2. Key Laboratory of Nonferrous Materials Science and Engineering of Ministry of Education, Central South University, Changsha 410083, China;
3. Nonferrous Metal Oriented Advanced Structural Materials and Manufacturing Cooperative Innovation Center, Central South University, Changsha 410083, China
4. Aerospace Research Institute of Materials and Processing Technology, Beijing 100076, China

Received 22 February 2018; accepted 26 May 2018

Abstract: The evolution and distribution of the aging precipitates in 1460 Al−Li alloy with high Li concentration (2.14%, mass fraction) during T6 aging and two-step T8 (4% predeformation) aging were investigated through TEM. The aging precipitates include δ' (Al_3Li) and $T1$ (Al_2CuLi) phases, of which the δ' phases are formed first in grain interiors. A lot of δ'/GPI/δ' composite precipitates in which GPI zones are flanked with a pair of δ' phases, are formed at 145 °C of T6 aging, which are thermally stable. At 160 °C and 175 °C of T6 aging, many $T1$ phases nucleate first at subgrain boundaries and grain boundaries, and then form and grow within grains. As to the T8 aging, the δ'/GPI/δ' composite precipitates are formed during the first-step aging at 130 °C for 20 h, which are thermally stable during the second-step aging at 160 °C. The plastic predeformation accelerates $T1$ nucleation within grains during the second-step aging at 160 °C.

Key words: Al−Li alloy; precipitate; T6 aging; T8 aging; aging temperature

1 Introduction

Li-containing Al alloys (Al−Li alloys) were considered as the most attractive alloys in the aircraft and aerospace industries because of their desirable properties, such as low density, high specific strength and elastic modulus, good corrosion resistance, excellent cryogenic properties, and low fatigue crack growth rate [1,2]. In fact, the third generation Al−Li alloys, such as 2195, 2050, 2099, 2196 and 2197 alloys were successfully used and performed excellently in aircraft and aerospace structures [1].

In addition to Li element, another main alloying element Cu is added, forming Al−Cu−Li series of Al−Li alloys. The precipitate type and precipitation process in Al−Cu−Li alloys are greatly enriched and much different from those in binary Al−Li alloys. The possible precipitates are transferred from individual δ' (Al_3Li) precipitate to those possibly including δ', GPI zones, GPII zones, θ' (Al_2Cu) and T1 (Al_2CuLi) precipitates [3−5]. Meanwhile, the precipitate type and fraction are highly dependent on the composition of Al−Li alloy, mainly Cu and Li concentrations and their ratio [6−8]. Due to the difference in crystal structure and the interface relation with the matrix, this precipitate type variation in turn results in a great difference in performance of alloy. On the other hand, the precipitate types and evolution are also associated with the aging temperature and aging process. Therefore, in addition to the performance of alloy, the Al−Li alloy microstructures related to compositions and aging process are always the research focus.

The Li concentration of most third generation Al−Li alloys and some other new developed Al−Li alloys, such as 2198, 2050, 2195 and 2055 alloys, was lower than 1.5%, their main strengthening precipitates were $T1$ and θ', and a lot of research was therefore focused on these Al−Li alloys [3,9−13]. However, there were also some Al−Li alloys with Li concentration higher than 1.5%,

Foundation item: Projection (2013AA032401) supported by the National High-Tech Research and Development Program of China
Corresponding author: Dan-yang LIU; Tel: +86-13278861206; E-mail: liudanyang@csu.edu.cn
DOI: 10.1016/S1003-6326(18)64910-6

such as 2099 and 2196 alloys, and the research on their microstructure evolution was much small. Actually, this kind of Al−Li alloy plays a greater role in weight saving, because of their higher Li concentration. Meanwhile, the precipitate types were more complicated in one specific alloy with high Li concentration, which possibly included δ', $T1$, GPI zones and θ'[14−17].

1460 Al−Li alloy was developed in Russia in 1960s. Due to its poor workability and low fracture toughness, this alloy has not attracted enough attention, and its precipitation behavior is still not fully known. However, it displayed good weldability [18] and excellent weight saving effect, due to its Li concentration higher than 2.0%. In China, it therefore attracted much attention in aerospace engineering recently, and some research was done on this alloy [19−22]. It was well known that the precipitate type and distribution could be modified through aging temperature variation and plastic predeformation, and accordingly the performance could be effectively enhanced. Moreover, due to the advantages in weight saving, the research on the Al−Li alloy with high Li concentration will be paid more attention in the near future. Therefore, the precipitation of 1460 Al−Li alloy at different temperatures and during different aging processes (T6 and T8) was systematically investigated in this case.

2 Experimental

The 1460 Al−Li alloy ingot was prepared through melting and casting, the raw materials included pure metals of Al, Cu, Li and intermediate alloys of Al−2%Sc, Al−4%Zr and Al−10%Ce (mass fraction). During this process, the melt was protected by Ar gas and flux. Its chemical composition is listed in Table 1. The ingot was rolled to sheet with 2 mm in thickness through hot rolling and cold rolling processes. After solid solution treatment and quenching in water, the sheet was then subjected to T6 aging at different temperatures (145, 160 and 175 °C) and a two-step T8 aging. The aging parameters are listed in Table 2. The chosen temperatures were usually used for Al−Li alloys with main aging precipitates of δ' and $T1$, and the corresponding tensile properties were previously measured [19,20].

The microstructures of the 1460 Al−Li alloy with different tempers were observed through using a Tecnai G^2 20 transmission electron microscope (TEM) operated at 200 kV. The TEM samples were prepared by a twin-jet electro-polishing device in a solution containing 75% methanol and 25% nitric acid (volume fraction) at −40 to 20 °C with a voltage of 15−30 V and a current of 70−95 mA. The observations were performed through selected area electron diffraction (SAED), dark field (DF) and bright field (BF) imaging models.

Table 1 Chemical composition of 1460 Al−Li alloy (mass fraction, %)

Cu	Li	Zr	Sc	Ce	Al
3.12	2.14	0.11	0.12	0.015	Bal.

Table 2 Aging parameters for 1460 Al−Li alloy

Aging	Predeformation/%	Temper
T6-1	0	145 °C, 0.5 h, 34 h, 116 h
T6-2	0	160 °C, 0.5 h, 29 h, 112 h
T6-3	0	175 °C, 0.5 h, 29 h, 112 h
T8	4	(130 °C, 20 h)+(160 °C, 12 h, 76 h)

3 Results

3.1 Microstructure after T6 aging

3.1.1 Aging at 145 °C

Figure 1 shows the $[100]_{Al}$ SAED patterns and TEM images of the 1460 Al−Li alloy aged at 145 °C for different time. As aged for 0.5 h, in the $[100]_{Al}$ SAED pattern, in addition to the spots of the matrix, only spots corresponding to δ' precipitates appear at $\{110\}_{Al}$ and $\{100\}_{Al}$. Accordingly, there exist a large number of δ' precipitates in the DF image viewed along $\langle 100\rangle_{Al}$ direction (Fig. 1(a)). As the aging time is extended to 34 h, in addition to the obvious δ' spots, there appear weak but continuous streaks passing through $\{200\}_{Al}$ and $\{110\}_{Al}$ spots, which indicates the formation a small fraction of GPI zones [23]. Accordingly, a large number of δ' precipitates (Fig. 2(b)) and some GPI zones (Fig. 2(c)) are observed in the DF and BF images taken along the $\langle 100\rangle_{Al}$ direction, respectively. Meanwhile, it is noted that the precipitated GPI zones are flanked by a pair of lenticular δ' precipitates (see insert in Fig. 2(b)) to form δ'/GPI/δ' composite precipitates.

As the aging time is further extended to 116 h, the spot types in the $[100]_{Al}$ SAED are not changed, but the intensity of the continuous streaks corresponding to the GPI zones is increased (Fig. 2(d)). In the DF image taken along the $\langle 100\rangle_{Al}$ direction, a great number of δ' precipitates are observed (Fig. 2(d)). Meanwhile, in the BF image taken along the $\langle 100\rangle_{Al}$ direction, much more GPI zones appear (Fig. 2(e)). In addition, all GPI zones are still flanked by a pair of lenticular δ' precipitates to form a lot of lenticular δ'/GPI/δ' composite precipitates (see insert in Fig. 2(d)). Actually, in all the aged samples, there always exist Al_3(Sc,Zr) dispersoids, which are formed during the annealing and thermo-mechanical process, but not during the aging process.

3.1.2 Aging at 160 °C

Figure 2 shows the SAED patterns and TEM images of the 1460 Al−Li alloy aged at 160 °C for different time. As aged for 0.5 h, the $[100]_{Al}$ SAED pattern shows that

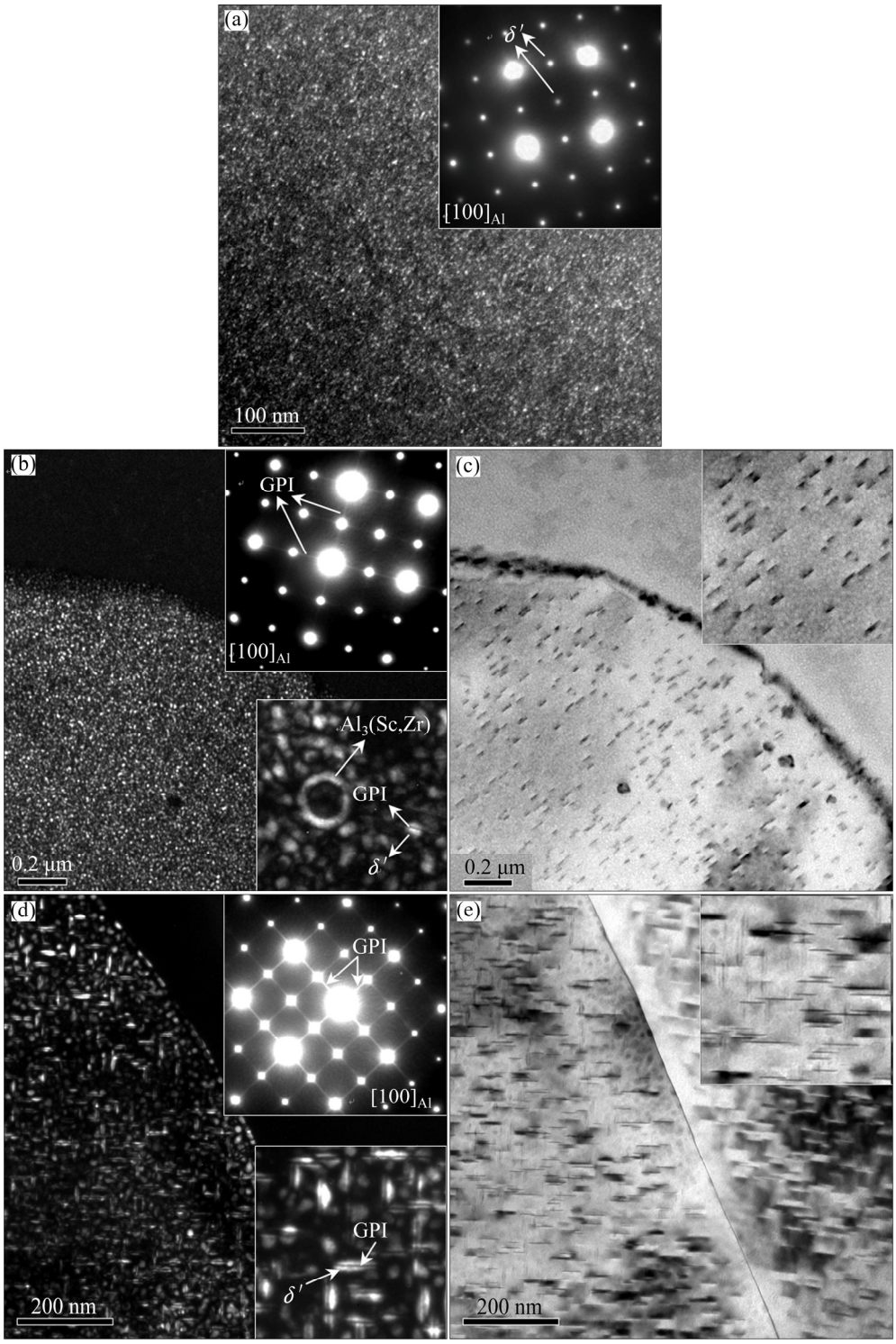

Fig. 1 TEM images and SAED patterns of 1460 Al−Li alloy after T6 aging at 145 °C for 0.5 h (a), 34 h (b, c) and 116 h (d, e): (a, b, d) $[100]_{Al}$ SAED patterns and DF images showing δ' precipitates taken along $\langle 100\rangle_{Al}$ direction; (c, e) BF images showing GPI zones taken along $\langle 100\rangle_{Al}$ direction

only δ' phases are precipitated, which are observed by the DF image taken along the $\langle 100\rangle_{Al}$ direction (Fig. 2(a)). As the aging time is extended to 29 h, the $[100]_{Al}$ SAED pattern and the DF image viewed along the $\langle 100\rangle_{Al}$ direction show a high fraction of δ' precipitates. In addition, it is noted that at subgrain boundaries, δ' phases are absent (Fig. 2(b)). Meanwhile, the streaks corresponding to GPI zones cannot be distinguished, but weak spots are observed at 1/3{220} and 2/3{220} in the $[100]_{Al}$ SAED pattern (dash circle in Fig. 2(b)), which means that $T1$ phases are formed. Some $T1$ precipitates are observed at subgrain boundaries in the DF image

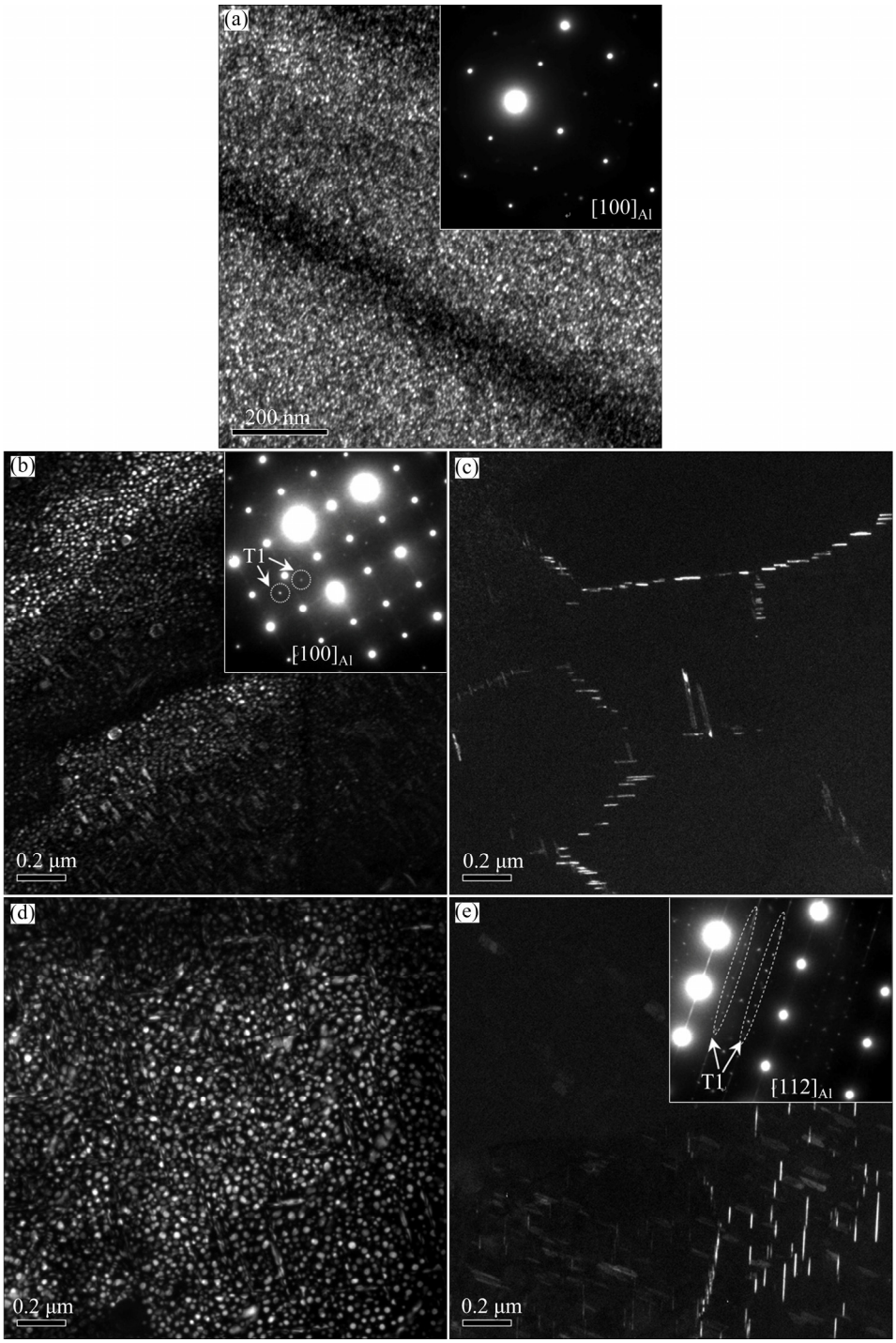

Fig. 2 TEM images and SAED patterns of 1460 Al−Li alloy after T6 aging at 160 °C for 0.5 h (a), 29 h (b, c) and 112 h (d, e): (a, b, d) $[100]_{Al}$ SAED patterns and DF images showing δ' precipitates taken along $\langle 100\rangle_{Al}$ direction; (c, e) $[112]_{Al}$ SAED pattern and DF images showing T1 precipitates taken along $\langle 112\rangle_{Al}$ direction

taken along the $\langle 112\rangle_{Al}$ direction (Fig. 2(c)). It is much important that *T*1 precipitates are sparse within grains (Fig. 2(c)).

As the aging time is further extended to 112 h, the δ' precipitates shown in the DF image viewed along the $\langle 100\rangle_{Al}$ direction are coarsened (Fig. 2(d)). Meanwhile, clear streaks passing through $1/3\{220\}_{Al}$ and $2/3\{220\}_{Al}$ spots are observed in the $[112]_{Al}$ SAED pattern, a lot of *T*1 precipitates therefore appear both within the grains and at the subgrain boundaries in the DF image viewed along the $\langle 112\rangle_{Al}$ direction (Fig. 2(e)).

3.1.3 Aging at 175 °C

Figure 3 shows the SAED patterns and TEM DF images of the 1460 Al−Li alloy after T6 aging at 175 °C

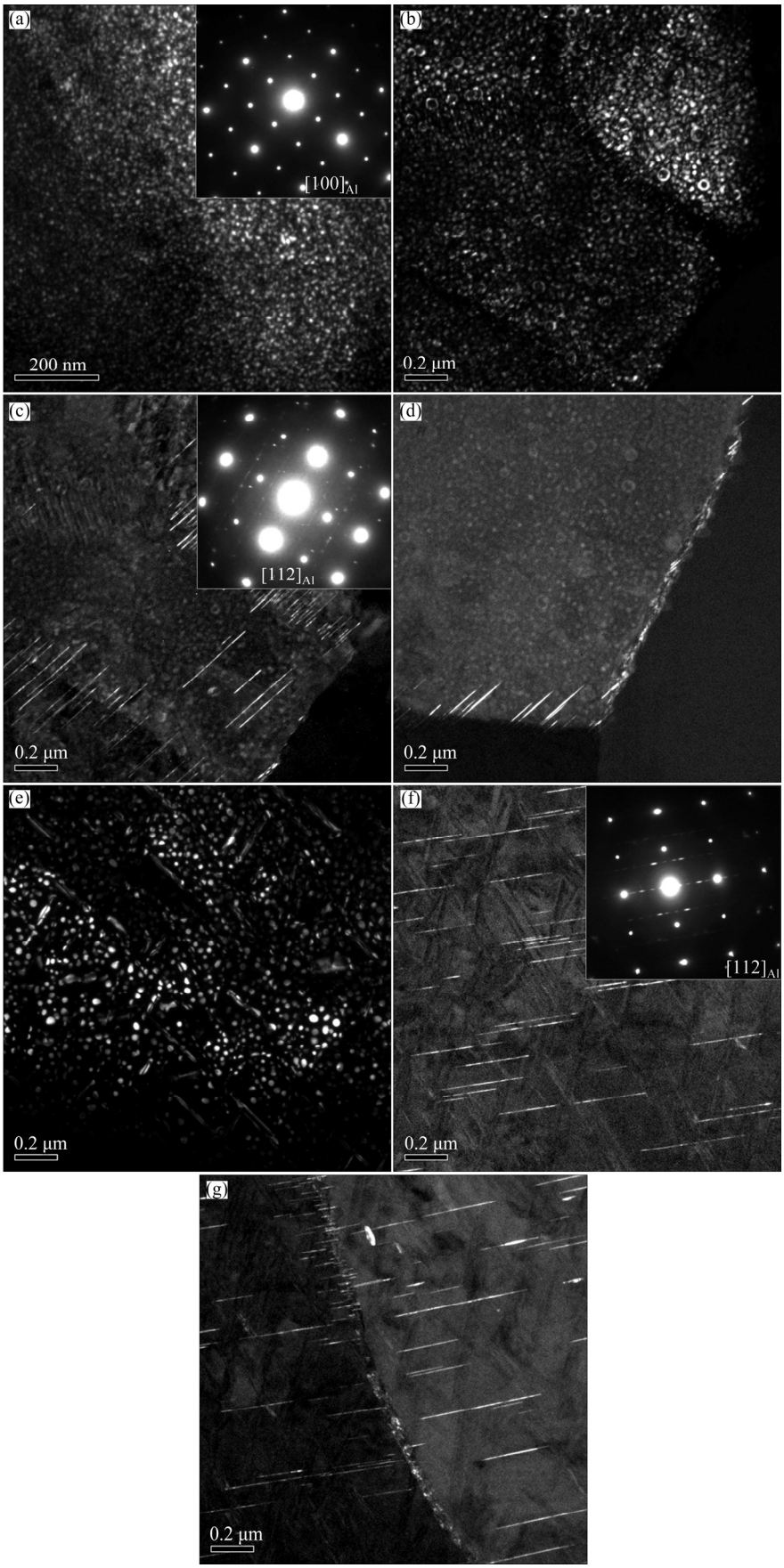

Fig. 3 TEM images and SAED patterns of 1460 Al−Li alloy after T6 aging at 175 °C for 0.5 h (a), 29 h (b, c, d) and 96 h (e, f, g): (a, b, e) $[100]_{Al}$ SAED pattern and DF images showing δ' precipitates taken along $\langle 100\rangle_{Al}$ direction; (c, d, f, g) $[112]_{Al}$ SAED patterns and DF images showing $T1$ precipitates taken along $\langle 112\rangle_{Al}$ direction

for different time. Only δ' phases are precipitated after aging for 0.5 h (Fig. 3(a)). After aging for 29 h, δ' precipitates are coarsened, which are mainly distributed within the grains and sparse at the subgrain boundaries and grain boundaries (Fig. 3(b)).

Meanwhile, $T1$ precipitates are observed, which are mainly distributed at the subgrain boundaries (Fig. 3(c)) and grain boundaries (Fig. 3(d)), and sparse within the grains. It is also noted that $T1$ precipitates at subgrain boundaries and grain boundaries extend to the grain interiors (Figs. 3(c) and (d)).

As the aging time is further extended to 96 h, the number density of δ' precipitates is lowered, and their size seems to increase a little (Fig. 3(e)). However, more intense streaks passing through $1/3\{220\}_{Al}$ and $2/3\{220\}_{Al}$ spots are observed in the $[112]_{Al}$ SAED patterns. Accordingly, $T1$ precipitates are massively formed within grains (Fig. 3(f)), and their amount is decreased at subgrain boundaries (Fig. 3(g)). In addition, compared to that in the sample aged at 160 °C, $T1$ number density in the sample aged at 175 °C is smaller.

3.2 Microstructure evolution during T8 aging

Figure 4 shows the SAED patterns and TEM images of the 1460 Al−Li alloy after T8 aging for different time. After the first-step aging at 130 °C for 20 h, massive δ' phases are precipitated (Fig. 4(a)). Meanwhile, weak streaks corresponding to GPI zones are observed to pass through $\{200\}_{Al}$ spots in the $[100]_{Al}$ SAED pattern. After the second-step aging at 160 °C for 12 h following the first-step aging at 130 °C for 20 h, in addition to the diffraction spots of δ' phases, intense continuous streaks passing through $\{200\}_{Al}$ and $\{110\}_{Al}$ spots are observed in the $[100]_{Al}$ SAED pattern (Fig. 4(b)), which indicates that many GPI zones are formed. Accordingly, many GPI zones are observed in the BF image taken along the $\langle 100\rangle_{Al}$ direction (Fig. 4(c)), which are also flanked by a pair of lenticular δ' precipitates (see insert in Fig. 4(b)). Furthermore, spots corresponding to $T1$ precipitates are observed in the $[112]_{Al}$ SAED pattern, and $T1$ precipitates are found both at the subgrain boundaries and within the grains (Fig. 4(d)).

As the second-step aging at 160 °C is extended to 76 h, δ' precipitates grow. Meanwhile the streaks passing through $\{200\}_{Al}$ and $\{110\}_{Al}$ spots in $[100]_{Al}$ SAED pattern break up (Fig. 4(e)), indicating that the GPI zones almost disappear and GPII zones (maybe include θ') form [23]. Similar to GPI zones, GPII zones also are flanked by a pair of lenticular δ' precipitates, forming δ'/GPII/δ' composite precipitates (see insert in Fig. 4(f)). In addition, $T1$ precipitates are massively precipitated within the grains, the number density of intragranular $T1$ precipitates is increased (Fig. 4(h)), but their amount at the subgrain boundaries is decreased (Fig. 4(g)).

4 Discussion

4.1 Effect of T6 aging temperature on precipitate distribution and evolution

According to the above observations, the precipitate types at different temperatures are different. Meanwhile, the precipitate distribution is also different as aged for different time. Table 3 lists the precipitates and their distribution in the alloys aged at different temperatures for different time. As aged for 0.5 h at all temperatures, the precipitates are uniform intragranular δ' phases. With aging time extension, the precipitate type and distribution are much different.

At the low temperature of 145 °C, GPI zones precipitate within grains, and form the δ'/GPI/δ' composite precipitates, which are thermally stable during aging for 34−116 h.

At the medium temperature of 160 °C, GPI zones are difficult to be distinguished. However, $T1$ precipitates are found to form at the subgrain boundaries as aged for 29 h. With the aging time extension, $T1$ phases are massively precipitated within grains.

At a higher temperature of 175 °C, GPI zones are not found. $T1$ phases also form at the subgrain boundaries and grain boundaries first, and then grow into the grain interiors. With aging time extension, the $T1$ precipitates form inside the grains, and their amount at the grain boundaries and subgrain boundaries is decreased. Compared to that aged at 160 °C, the difference lies in that the aging response is accelerated, but the number density of the $T1$ precipitates is lowered.

The above observations show following features: (1) δ' phases show a much shorter incubation time than $T1$ phases, therefore precipitate quickly from the matrix. (2) It is unique and of interest that at low temperature of 145 °C, the δ'/GPI/δ' composite precipitates are formed, which are stable during a long time of aging. (3) $T1$ phases are precipitated at 160 °C and 175 °C, but not at 145 °C. (4) $T1$ phases are precipitated at subgrain boundaries and grain boundaries first, then within grains.

The precipitation behavior of the 1460 Al−Li alloy aged at 145 °C is much different from the precipitation of Al−Cu−Li alloys with low Li concentration, such as 2195 and 2050 Al−Li alloys. MA et al [13] investigated the precipitation in the 2195 Al−Li alloy during T8 aging at 145 °C. At aging stage (15 h), the GPII zones were found. However, as the aging time was extended to 60 h, the GPII zones disappeared and θ' precipitates were observed. In this case, for the 1460 Al−Li alloy, the GPI zones are thermally stable and still exist, though the aging time at 145 °C is extended to 116 h. This precipitation behavior should be related to its composition and the early microstructure.

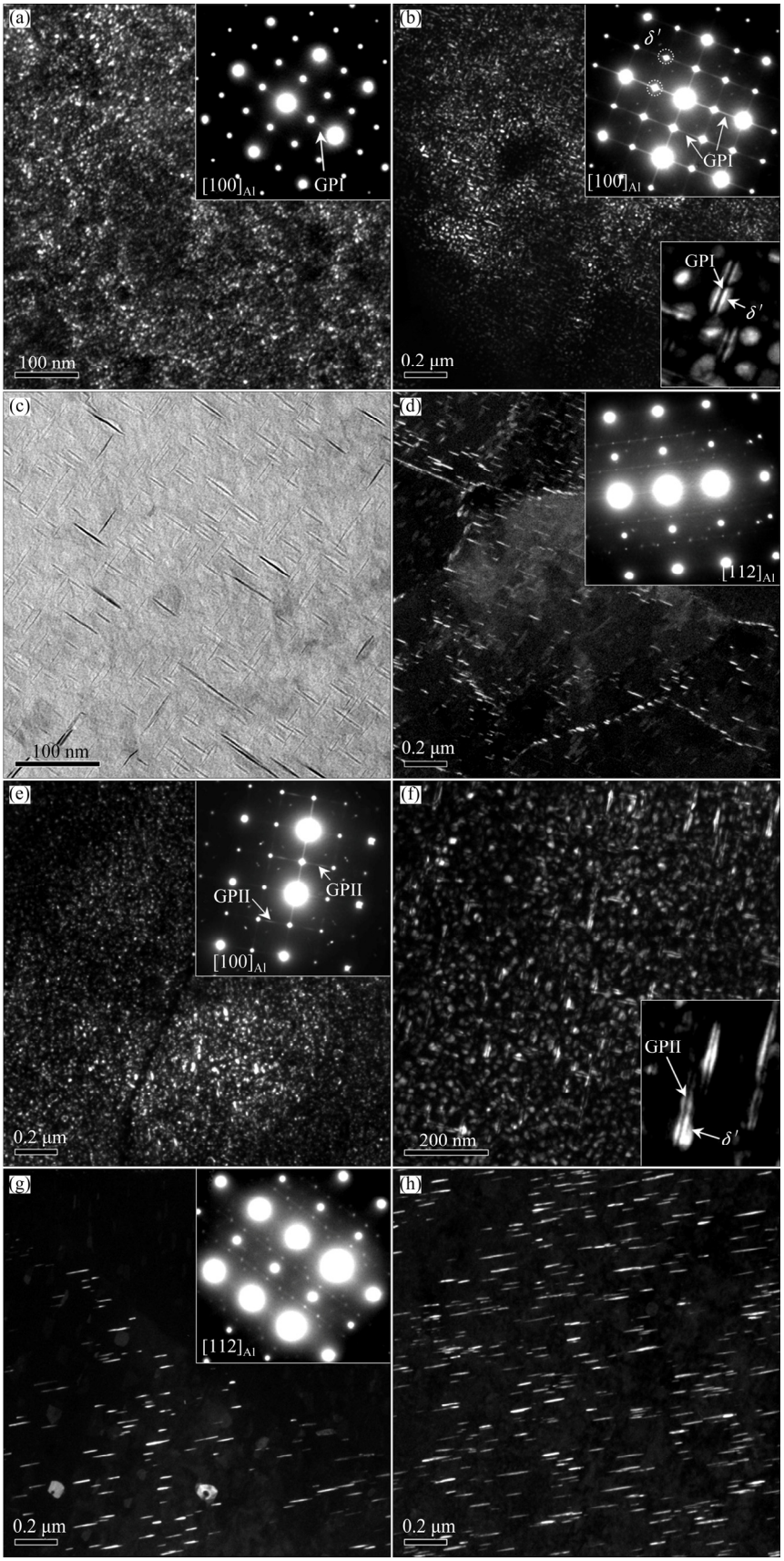

Fig. 4 TEM images and SAED patterns of 1460 Al−Li alloy after T8 aging including 130 °C, 20 h (a), (130 °C, 20 h)+(160 °C, 12 h) (b, c, d) and (130 °C, 20 h)+(160 °C, 76 h) (e, f, g, h): (a, b, e, f) $[100]_{Al}$ SAED patterns and DF images showing δ' precipitates taken along $\langle 100\rangle_{Al}$ direction; (c) BF image showing GPI zones taken along $\langle 100\rangle_{Al}$ direction; (d, g, h) DF images showing $T1$ precipitates taken along $\langle 112\rangle_{Al}$ direction

Table 3 Precipitates and distribution during T6 aging at different temperatures for different time

Temperature/ °C	0.5 h	29−34 h		96−116 h	
		Precipitate	Distribution	Precipitate	Distribution
145	δ'	δ'	GI	δ'	GI
		δ''/GPI/δ'	GI	δ''/GPI/δ	GI
160	δ'	δ'	GI	δ'	GI
		$T1$	SGB, GB	$T1$	SGB, GB, GI
175	δ'	δ'	GI	δ'	GI
		$T1$	SGB, GB	$T1$	SGB, GB, GI

Note: GI=grain interior; SGB=subgrain boundary; GB=gain boundary

The 1460 Al−Li alloy is featured with a high Li concentration (2.14%) and a low Cu/Li mass ratio. This composition feature determines a much great thermodynamic driving force for δ' preferential precipitation. In addition, δ' precipitates and GPI zones are coherent with the Al matrix and possess much small interfacial energy of 0.014 J/m^2 [24] and 0.003 J/m^2 [25]. The high coherency and much small interfacial energy stimulate the formation of δ' precipitates and GPI zones at the early aging stage.

It is critical that the δ''/GPI/δ' composite precipitates are formed during the aging at 145 °C. This can be answered by considering strain fields around the GPI zones. Due to the difference in the lattice constants of Al (0.405 nm) and fcc Cu (0.361 nm), the Al matrix in the vicinity of GPI zones should be subject to a compressive stress. In addition, the lattice constant of the δ' phase (0.4038 nm) is a little lower than that of the matrix. Therefore, it can be anticipated that the δ' phase around the GPI zones effectively acts as a buffer layer to accommodate the large strain [14]. Accordingly, as the GPI zones are formed, the δ' phase can nucleate and grow on the GPI zones. This structure can effectively minimize the energy barrier of δ' nucleation. First principles calculations also confirmed that forming the δ''/GPI/δ' composite phase was more energetically favored than forming the individually separate δ' phase and GPI zone [26]. Longer time aging leads to well-developed structures of GPI zones flanked by a pair of lenticular δ' particles, making the overall shape an oblate spheroid and forming δ''/GPI/δ' composite precipitates.

Once the δ''/GPI/δ' composite precipitates are formed, they are stabilized. The thermal stability of the resultant structure most likely originates from the minimization of stress due to the lattice mismatch among the Al matrix, GPI zone, and the δ' phase [14].

It is well known that the preferential precipitates in Al−Cu alloys depends on the Cu concentration and temperature. Lower aging temperature and higher Cu concentration favor the preferential precipitation of GPI zones, but higher aging temperature is not favorable for the formation of GPI zones. Therefore, as aged at temperatures higher than 160 °C, GPI zones are not formed, but $T1$ precipitates are precipitated instead, the aging precipitates consist of δ' and $T1$. An important feature is that $T1$ precipitate is distributed first at the subgrain boundaries and grain boundaries, but δ' within the grain. With aging time extension, $T1$ precipitate forms and grows within the grains. This distribution feature is associated with the different characteristics of $T1$ and δ' precipitates. δ' precipitates are coherent with the Al matrix and possess a much small interfacial energy of 0.014 J/m^2, but $T1$ precipitates are semi-coherent with the matrix and possess a higher interfacial energy of 0.13−0.23 J/m^2 [8]. During solid state transformation, it is necessary to overcome or minimize the energy barrier for nucleation. For a given local super-saturation at a given site, the energy barrier depends on the misfit strain energy and interfacial energy. The energy barrier for $T1$ nucleation is therefore much higher than that for δ' nucleation. To overcome or minimize the resistance or energy barrier, $T1$ precipitates prefer to nucleate at the sites of dislocation, grain boundary, subgrain boundary, stacking fault and vacancy cluster. Therefore, in the 1460 Al−Li alloy, $T1$ precipitates nucleate more easily at the grain boundaries first, but δ' precipitates nucleate within the grains.

4.2 Effect of T8 aging on precipitate distribution and evolution

After the T8 second-step aging at 160 °C, in addition to the δ' precipitates, both the δ''/GPI/δ' composite precipitates and $T1$ precipitates are formed, and the precipitation kinetics of intragranular $T1$ precipitates is higher than that during T6 aging at 160 °C. This precipitation behavior is determined by the following two factors during the T8 aging.

The first factor is the first-step aging at low temperature of 130 °C for 20 h prior to the second-step aging at 160 °C. The second is the small plastic predeformation. The low temperature (130 °C) aging for

20 h leads to the formation of GPI zones and δ' precipitates (see SAED pattern in Fig. 4(a)). Although the GPI zones flanked by a pair of δ' precipitates were not observed by TEM DF image in this case, this phenomenon was detected in Al−3.2Cu−(1.6−2.4)Li alloys aged at 100 °C for 1 d through HRTEM [14]. Considering that GPI zones form according to the $[100]_{Al}$ SAED pattern in the sample aged at 130 °C for 20 h, and the δ''/GPI/δ' composite precipitates are formed as aged at 145 °C for 34 h (Figs. 2(b) and (c)), it is rational that the δ''/GPI/δ' composite precipitates are formed after aging at 130 °C for 20 h. This composite structure is thermally stable during the second-step aging at 160 °C. Similar phenomenon was found in the Al−3.2Cu−2.4Li and Al−3.2Cu−1.6Li alloys during a two-step T6 aging [14]. The δ''/GPI/δ' composite precipitates were formed in these two alloys after the first-step aging at 100 °C for 1 d. Due to the minimization of stress caused by the lattice mismatch among the Al matrix, GPI zone, and the δ' phase, the δ''/GPI/δ' composite precipitates were thermally stable and still existed after the second-step aging at a high temperature of 190−200 °C for 2 or 3 d [14].

The small plastic predeformation plays an important role in controlling the *T*1 precipitation. According to the TEM observations, the intragranular *T*1 precipitation kinetics is much faster during T8 aging than that during T6 aging at 160 °C. After 12 h of the second-step T8 aging at 160 °C, *T*1 phases are formed not only at the subgrain boundaries and grain boundaries, but also within the grains (Fig. 4(d)). However, after T6 aging at 160 °C for 29 h, *T*1 phases are mainly precipitated at the subgrain boundaries and grain boundaries, and are absent within the grains (Fig. 2(c)). This is associated with the intragranular dislocations caused by plastic pre-deformation which provide nucleation sites for the *T*1 precipitates. The nucleation barrier of the semi-coherent *T*1 precipitates is decreased as they nucleate on the dislocations [8].

5 Conclusions

(1) For all tempers, the main precipitates are intragranular δ' phases which are precipitated at the early aging stage.

(2) At 145 °C of T6 aging, a lot of intragranular δ''/GPI/δ' composite phases in which GPI zones are flanked with a pair of lenticular δ' phases, are formed, which are thermally stable and still exist after aging for a long time of 116 h.

(3) At 160 °C and 175 °C of T6 aging, *T*1 phases nucleate first at the subgrain boundaries and grain boundaries, then form and grow in the grain interiors.

(4) During the two-step T8 aging, the low temperatures (130 °C) of the first-step aging results in the formation of δ''/GPI/δ' composite precipitate, which are thermally stable during the following second-step aging at 160 °C. In addition, the plastic deformation accelerates the uniform nucleation of intragranular *T*1 precipitates.

References

[1] RIOJA R J, LIU J. The evolution of Al−Li base products for aerospace and space applications [J]. Metallurgical Materials Transaction A, 2012, 43(9): 3325−3337.

[2] ZHENG Zi-qiao, LI Jin-feng, CHEN Zhi-guo, LI Hong-ying, LI Shi-chen, TAN Cheng-yu. Alloying and microstructural evolution of Al−Li alloys [J]. The Chinese Journal of Nonferrous Metals, 2011, 21(10): 2337−2351 (in Chinese)

[3] LI Jin-feng, YE Zhi-hao, LIU Dan-yang, CHEN Yong-lai, ZHANG Xu-hu, XU Xiu-zhi, ZHENG Zi-qiao. Influence of pre-deformation on aging precipitation behavior of three Al−Cu−Li alloys [J]. Acta Metallurgica Sinica (English Letters), 2017, 30(2): 133−145.

[4] DECREUS B, de GEUSER F, DESCHAMPS A, DONNADIEU P, SIGLI C. Precipitation sequence in two Al−Li−Cu alloys [J]. Solid State Phenomenon, 2011, 172−174: 267−272.

[5] GAO Zhen, CHEN Jiang-hua, DUAN Shi-yun, YANG Xiu-bo, WU Cui-lan. Complex precipitation sequences of Al−Cu−Li−(Mg) alloys characterized in relation to thermal ageing processes [J]. Acta Metallurgica Sinica (English Letters), 2016, 29(1): 94−103.

[6] DECREUS B, DESCHAMPS A, GEUSER F De, DONNADIEU P, SIGLI C, WEYLAND M. The influence of Cu/Li ratio on precipitation in Al−Cu−Li−x alloys [J]. Acta Materialia, 2013, 61: 2207−2218.

[7] LI Jin-feng, LIU Ping-li, CHEN Yong-lai, ZHANG Xu-hu, ZHENG Zi-qiao. Microstructures and mechanical properties of Mg, Ag and Zn multi-microalloyed Al−(3.2−3.8)Cu−(1.0−1.4)Li alloys [J]. Transactions of Nonferrous Metals Society of China, 2015, 25(7): 2103−2112.

[8] GABLE B M, ZHU A W, CSONTOS A A, STARKE Jr E A. The role of plastic deformation on the competitive microstructural evolution and mechanical properties of a novel Al−Li−Cu−X alloy [J]. Journal of Light Metals, 2001, 1: 1−14.

[9] HUANG B P, ZHENG Z Q. Independent and combined roles of trace Mg and Ag additions in properties, precipitation process and precipitation kinetics of Al−Cu−Li−(Mg)−(Ag)−Zr−Ti alloys [J]. Acta Materialia, 1998,46(12): 4381−4393.

[10] BALDUCCI E, CESCHINI L, MESSIERI S, WENNER S, HOLMESTAD R. Effects of overaging on microstructure and tensile properties of the 2055 Al−Cu−Li−Ag alloy [J]. Materials Science and Engineering A, 2017, 707: 221−231.

[11] ARAULLO-PETERS V, GAULT B, GEUSER F De, DESCHAMPS A, CAIRNEY J M. Microstructural evolution during ageing of Al−Cu−Li−X alloys [J]. Acta Materialia, 2014, 66: 199−208.

[12] GAO C, MA Y, TANG L Z, WANG P, ZHANG X. Microstructural evolution and mechanical behavior of friction spot welded 2198-T8 Al−Li alloy during aging treatment [J]. Materials & Design, 2017, 115: 224−230.

[13] MA Yun-long, LI Jin-feng, LIU Guan-ri, LIU Dan-yang, YE Zhi-hao, WANG Jie-xia, ZHENG Zi-qiao. Microstructural evolution and mechanical properties of 2195 Al−Li alloy during T8 re-aging at various temperatures following re-solution [J]. The Chinese Journal of Nonferrous Metals, 2017, 27(2): 234−242. (in Chinese)

[14] YOSHIMURA R, KONNO T J, ABE E, HIRAGA K. Transmission electron microscopy study of the early stage of precipitates in aged

Al−Li−Cu alloys [J]. Acta Materialia, 2003, 51: 2891−2903.
[15] YOSHIMURA R, KONNO T J, ABE E, HIRAGA K. Transmission electron microscopy study of the evolution of precipitates in aged Al−Li−Cu alloys: The θ' and $T1$ phases [J]. Acta Materialia, 2003, 51: 4251−4266.
[16] AHMADI S, ARABI H, SHOKUHFAR A. Formation mechanisms of precipitates in an Al−Cu−Li−Zr alloy and their effects on strength and electrical resistance of the alloy [J]. Journal of Alloys and Compounds, 2009, 484: 90−94.
[17] MA Y, ZHOU X, THOMPSON G E, HASHIMOTO T, THOMSON P, FOWLES M. Distribution of intermetallics in an AA 2099-T8 aluminium alloy extrusion [J]. Materials Chemistry and Physics, 2011, 126: 46−53.
[18] FRIDLYANDER I N, DRITS A M, KRYMOVA T V. Possibility of creating weldable alloys on the basis of the system Al−Cu−Li [J]. Metal Science and Heat Treatment, 1991, 33(9): 695−699.
[19] LIN Xiao-hong, LI Jin-feng, CHEN Yong-lai, ZHANG Xu-hu, XU Xiu-zhi, ZHENG Zi-qiao. Tensile properties and microstructure of 1460 Al−Li alloy sheet aged at different temperatures [J]. Chinese Journal of Rare Metals, 2017, 41(12): 1293−1298. (in Chinese)
[20] LI Jin-feng, CHEN Yong-lai, ZHANG Xu-hu, XU Xiu-zhi, ZHENG Zi-qiao. Mechanical properties and microstructure of 1460 Al−Li alloy [J]. Journal of Central South University (Science and Technology), 2017, 48(11): 2866−2872. (in Chinese)
[21] MA Juan, YAN De-sheng, RONG Li-jian, LI Yi-yi. Effect of Sc addition on microstructure and mechanical properties of 1460 alloy [J]. Progress in Natural Science: Materials International, 2014, 24(1): 13−18.
[22] MA Juan, YAN De-sheng, RONG Li-jian, LI Yi-yi. Effect of aging on the microstructure and mechanical properties of 1460 alloy [J]. Acta Metallurgica Sinica (English Letters), 2015, 28(4): 454−459.
[23] WANG S C, STARINK M J. Precipitates and intermetallic phases in precipitation hardening Al−Cu−Mg−(Li) based alloys [J]. International Materials Reviews, 2005, 50(4): 193−215.
[24] BAUMANN S F, WILLIAMS D B. A new method for the determination of the precipitate−matrix interfacial energy [J]. Scripta Metallurgica, 1984, 18: 611−616.
[25] LOECHTE L, GIFT A, GOTTSTEIN G, HURTADO I. Simulation study on the evolution of the GP zones in Al−Cu alloys: An extended Cahn-Hilliard approach [J]. Acta Materialia, 2000, 48: 2969−2984.
[26] DUAN S Y, WU C L, GAO Z, CHA L M, FAN T W, CHEN J H. Interfacial structure evolution of the growing composite precipitates in Al−Cu−Li alloys [J]. Acta Materialia, 2017, 129: 352−360.

高 Li 含量 Al−Cu−Li 合金时效析出相的分布与演化

李劲风[1,2,3]，黄嘉蕾[1]，刘丹阳[1]，陈永来[4]，张绪虎[4]，马鹏程[4]

1. 中南大学 材料科学与工程学院，长沙 410083；
2. 中南大学 有色金属材料科学与工程教育部重点实验室，长沙 410083；
3. 中南大学 有色金属先进结构材料与制造协同创新中心，长沙 410083；
4. 航天材料及工艺研究所，北京 100076

摘　要：采用透射电镜研究高 Li 含量(2.14%，质量分数)1460 铝锂合金 T6(145、160、175 °C)及 T8 双级时效(4%预变形，130 °C，24 h+160 °C)时析出相的演化及分布。合金的时效析出相包括δ'(Al_3Li)相和 $T1$(Al_2CuLi)相，其中δ'相为晶内优先析出相。低温(145 °C)T6 时效时，晶内还形成大量均匀分布而且稳定的δ'/GPI/δ'复合相。较高温度(160 °C 及 175 °C) T6 时效时，还会析出大量 $T1$ 相；$T1$ 相优先于(亚)晶界形核，而后随时效时间延长，逐渐在晶内析出。T8 双级时效时，晶内可形成δ'/GPI/δ'复合相及 $T1$ 相；其中δ'/GPI/δ'复合相开始形成于第一级低温时效，并于第二级较高温度时效时一直稳定存在；$T1$ 相则形成于第二级时效，且 T8 时效时的预变形促进 $T1$ 相在晶内快速析出。

关键词：铝锂合金；析出相；T6 时效；T8 时效；时效温度

(Edited by Xiang-qun LI)